buildings

MDPI

Article

Risk Assessment of Road Blockage after Earthquakes

Luigi Sorrentino and Linda Giresini *

Department of Structural and Geotechnical Engineering, University of Rome La Sapienza, 00184 Rome, Italy; luigi.sorrentino@uniroma1.it
* Correspondence: linda.giresini@uniroma1.it

Abstract: This paper presents a safety tool to assess the risk of road blockage during and after emergency situations, mainly due to earthquakes. This method can be used by public authorities to calculate the risk of road paths prone to blockage in case of seismic events. Typological classes of elements interfering with roads, such as unreinforced masonry and reinforced concrete buildings, unreinforced masonry and reinforced concrete bridges, retaining walls, and slopes, are considered. The mean annual frequency (MAF) of exceedance of a blockage limit state is calculated for a path with redundant road segments considering fragility curves from the literature. A practical example is presented for Amatrice, a town in Central Italy hit by the 2016 earthquake. After verifying that the MAF of exceedance demand is lower than the capacity for two roads, a strengthening solution is assumed for two buildings in the path, resulting in a reduction by more than 50% of the MAF demand. For a higher safety level, a bypass is proposed obtaining a demand/capacity ratios four orders of magnitude lower than that obtained with strengthening solutions, highlighting and quantifying the beneficial effect of removing vulnerable structures along the path.

Keywords: earthquake; safe path; road blockage; bridges; retaining walls; slopes

check for updates

Citation: Sorrentino, L.; Giresini, L. Risk Assessment of Road Blockage after Earthquakes. *Buildings* **2024**, *14*, 984. https://doi.org/10.3390/buildings14040984

Academic Editor: Xavier Romão

Received: 17 February 2024
Revised: 29 March 2024
Accepted: 31 March 2024
Published: 2 April 2024

Copyright: © 2024 by the authors. Licensee MDPI, Basel, Switzerland. This article is an open access article distributed under the terms and conditions of the Creative Commons Attribution (CC BY) license (https://creativecommons.org/licenses/by/4.0/).

1. Introduction

The occurrence of natural disasters such as earthquakes, landslides, floods, volcanic eruptions, and hurricanes may cause severe damage to transportation systems, which are essential in guaranteeing access to sites and services as well as connection between people [1–4]. The falling of trees, signaling systems, lighting, and electric poles as well as debris from adjacent constructions may generate the blockage of a road segment. Those natural hazards can also engender direct damage on a road network, such as failure of road structural (e.g., bridges or tunnels) and non-structural components (metal culverts and pipelines) or soil failure/liquefaction with different grades of damage [5]. The consequent road blockage might isolate people and sites; during emergency situations, it hinders rescue and evacuation operations. In the long term, the blockage of a road causes human and economic losses for entire communities that could last for years. For these reasons, the assessment of the risk caused by the blockage of a road segment during natural hazards is a topic of primary concern for local authorities and road operators. The seismic risk assessment associated with the blockage of a redundant road connection between two points is the main objective of this study. This topic is very broad and involves risk models of different types of infrastructures. First, one should distinguish between risk models involving the blockage of roads due to individual failures (for example, the falling of debris from damaged buildings [6]) and risk models accounting for the blockage of an entire road network connecting at least two nodes [7].

When one considers a road network, the issue becomes more complicated inasmuch as the interaction between different road components and adjacent buildings or services implies combined probability of failures. Once the probability of failure of each structure (e.g., bridges) under an earthquake of given intensity is known, the topology of the road network allows to assess its reliability, that is, the probability of maintaining the connection

between the source node and the destination node [8]. Franchin et al. [9] presented a reliability analysis to estimate the effectiveness of rescue services considering the possible failure of bridges, schools, and hospitals after an earthquake. More recently, a method to assess the functionality of a road network in historical centers was proposed by Zanini et al. [10]. In it, the failure of unreinforced masonry building façades (local out-of-plane mechanisms [11]) was considered as a cause of road network blockage, and the percentage of obstructed road was calculated by means of probabilistic and fuzzy logic analyses. Another methodology compared duration and length of trips calculated for undamaged network conditions and for network disrupted after earthquakes [12]. The probability of a specific road being blocked is then combined with its number of users to assess the average number of affected vehicles and to identify the most critical segments. Other works considered road blockage due to co-seismic landslides [13], people flow under ordinary conditions and evacuations [14], buildings collapse due to tsunamis, and consequent evacuations [15,16]. All these contributions do not consider road blockage due to different types of interfering elements, which is then an original feature of this work. Indeed, to the authors' knowledge, no global models able to easily predict road blockage risk due to earthquakes in a path with different types of adjacent constructions and soil mechanisms have been previously presented. This paper therefore proposes a comprehensive and effective but simplified tool to estimate the seismic risk associated with road blockage considering all the main types of man-made and natural elements present along the paths. The main purpose of the study is allowing public authorities and road operators to estimate rapidly and with limited knowledge the seismic risk of a road network connecting two points as well as to explore alternative intervention scenarios when the computed risk is considered too high. Road blockage risk is particularly relevant when multiple small settlements are distributed in a vast territory, as is the case of Amatrice, a municipality struck by the 2016 Central Italy earthquake. The procedure does not account for abandoned vehicles or people flow during evacuations because the small settlements of internal Italian areas have a limited traffic level, and there are usually proper parking areas. Similarly, no blockage due to urban furniture is considered because no relevant observation was made during the 2016 Central Italy earthquakes. In any case, these aspects could be investigated in future developments of the research considering appropriate risk models such as those presented in Ito et al. (2020) and Takabatake et al. (2022).

Section 2 illustrates the proposed methodology, discussing the steps of the procedure to calculate the mean annual frequency (MAF) of exceedance of a road blockage limit state (LS). Section 3 describes the fragility and risk analysis, detailing the fragility curves selected for each class of elements influencing the road blockage (unreinforced masonry and reinforced concrete buildings, unreinforced masonry and reinforced concrete bridges, retaining walls on different soil types, slopes on different soil types, and different inclinations). It also explains how the MAF of exceedance of the road blockage LS of an individual road and of a redundant road connecting two points is calculated. Section 4 applies the proposed methodology to an explanatory road path in Amatrice, presenting all the steps of the calculations in tabular form to allow the reader to replicate them and fully understand the suggested procedure. After the assessment of seismic risk on two alternative paths, the risk assessment is deepened by discussing the impact of strengthening interventions on some of the buildings along the path and considering bypasses along the road.

2. Methodology

2.1. General Aspects and Objectives

The proposed methodology considers the interference between buildings (Figure 1), bridges, retaining walls, and slopes (hereinafter referred to as "interfering elements") damaged by an earthquake on the road. The relevance of this topic is clear when observing the performance of such elements in the 2016 Central Italy earthquake (Figure 2).

In this section, the MAF of exceedance of the road blockage LS is estimated by means of fragility curves considering the actual configuration of the road path. The fragility curves

are derived from the existing literature for typological classes of interfering elements, only adapting the curves to a common hazard framework when necessary. Each fragility curve delivers a probability of exceeding a considered LS conditioned to a hazard intensity. In the mentioned publications, further details are available about the empirical or analytical procedure used to derive the functions as well as on the different sources of uncertainties.



(**a**) (**b**)

Figure 1. Blockage of the main road of Retrosi settlement, which connects it with the adjacent settlements, due to seismic damage of an unreinforced masonry building (Amatrice municipality, 2016): (**a**) before and (**b**) after the earth-quake.



(**a**) (**b**)

Figure 2. (**a**) Damaged "Ponte a Tre Occhi" bridge and (**b**) landslide on road SR260 after the 2016 Central Italy earthquake.

2.2. Steps of the Procedure

The proposed procedure is meant for direct application by a technical employee of a public body or a road management entity by resorting to web-available data and elaborating the data into a spreadsheet. It consists of the following steps graphically shown in the flow chart of Figure 3:

1. Definition of a starting point;
2. Definition of an end point;
3. Identification of the possible connections, which can include two or more alternative (and therefore redundant) paths and then discretization of the path in road segments between two nodes;
4. Identification of interfering elements along each road segment, such as buildings, bridges, retaining walls, and slopes, each of which has its own fragility curve (the possible damage on the road itself is assumed to be negligible);
5. Definition of the seismic hazard of each element, accounting for the local seismic site response;
6. Calculation of the MAF of exceedance of the blockage LS due to each single element;

7. Calculation of the MAF of exceedance of the blockage LS associated to the entire path.

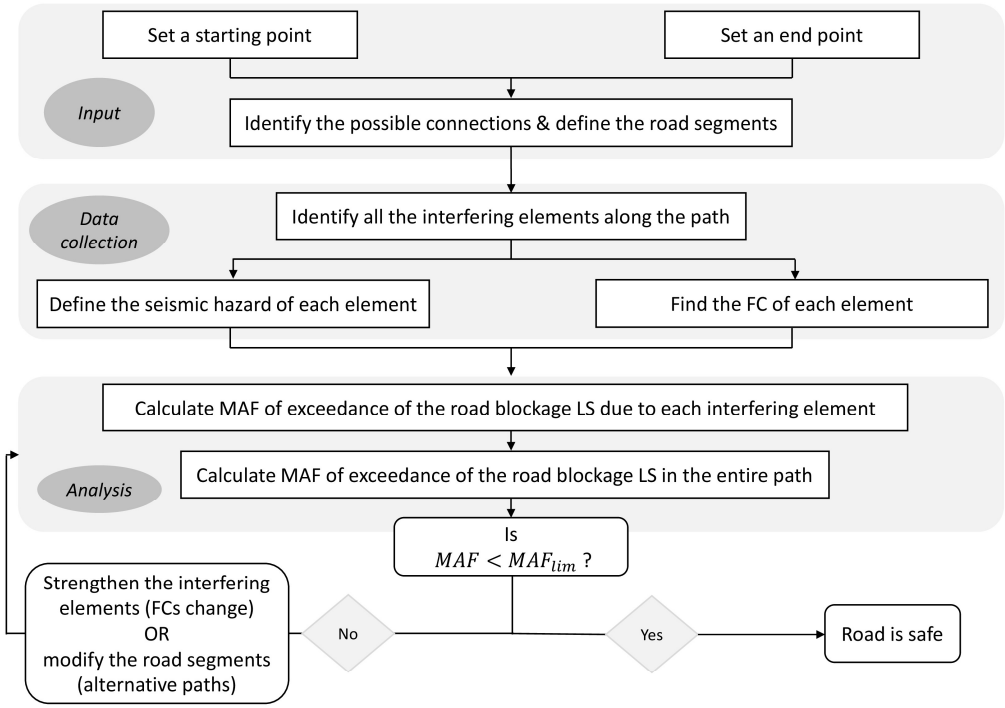

Figure 3. Flow chart of the proposed procedure.

The proposed analysis process is performed considering a path with a unique starting point and a unique end point. The blockage risk should be determined by considering, for each element, scenario analyses with magnitude, distance pairs, and attenuation laws. Nevertheless, such an approach appears to be unsuitable for its use by a small-scale technical office, which needs straightforward and easy-to-use assessment tools. In the end, a sophisticated tool would be unnecessary due to the great simplifications considered both in the vulnerability assessment and in the road layout. Hence, the code hazard curves, considering a uniform hazard at the municipality level, are used to calculate the MAF of exceedance of the LS. This frequency is finally compared to the following:

- An upper limit of MAF for the road blockage LS (capacity);
- A MAF of an alternative road due to the following:
  - (a) Reduction in the vulnerability of one or more elements along the path;
  - (b) Modification of the layout of one or more road segments, for instance, bypassing some critical points.

For what concerns the upper limit of MAF, there are no established values in the scientific community. The blockage LS of the road path can be associated with a severe damage of the interfering elements, for which one can assume a frequency of 5×10^{-4}, greater than the frequency of 2×10^{-4} considered for the near-collapse LS of consequence class 2 (ordinary) constructions ([17], Annex F therein). An even greater value can be assumed when dealing with existing structures ([18], note in Section 4.1(4) therein). In the application illustrated in Section 4.5, a value of 7×10^{-4} is assumed for each interfering element, and the road capacity is then computed accordingly. As for the alternative road, the MAF is determined by using the same procedure used for the original road but accounting for the interfering elements present therein (Figure 3).

3. Fragility and Risk Analysis

3.1. Fragility Curves for Buildings

A road blockage can be caused by the falling of debris—triggered by an earthquake—from buildings facing the road. Several studied have focused on the prediction of the debris-

falling distance from the footprint of buildings facing roads, considering remote sensing monitor technology [19], omnidirectional buffer debris models [20], probabilistic [21,22] and statistical [7] models based on observed data, as well as geometrical models. Geometrical models predict the debris distance as a function of the building dimensions and volume assuming a simplified shape of the collapsed building [2,7,23,24]. As discussed by Yu and Gardoni [6], geometrical models have two main limitations: (i) They neglect the influence of road design on the ability of the road to accommodate vehicles and (ii) arbitrarily assume a probability distribution to assess the probability of road blockage. Recently, to overcome such limitations Yu and Gardoni [6] proposed a novel mathematical formulation of a probabilistic model for predicting debris distance from damaged buildings, calibrating the model using a Bayesian approach and data from the 2010 Haiti earthquake.

However, to keep the model simple enough to be managed by a technical office with limited manpower, in the present work, the probability of road congestion caused by building damage is assumed equal to the probability of building damage, as carried out by Lo et al. [23]. The condition of interference between buildings is defined according to the geometric relationship [25]:

$$\frac{h_{b1} + h_{b2}}{w} \geq 1.0 \quad (1)$$

where h_{b1} is the eave height of the building to the left of the cross-section of the considered path (equal to zero if there is no building); h_{b2} is the eave height of the building to the right of the cross-section of the considered path (equal to zero if there is no building); w is the width of the path. For the value of w, one should also consider the possible recessed position of the building, as this case is beneficial for the path safety.

The fragility curves used in the method proposed herein are those derived empirically by Zucconi et al. [26] for unreinforced masonry buildings and by Del Gaudio et al. [27] for reinforced concrete buildings. For both building materials, the probability is evaluated by means of a lognormal distribution as a function of peak ground acceleration (PGA), assumed hereinafter as the product $a_g S$ (maximum site horizontal acceleration amplified by the site factor, with the former available in the Italian building code hazard [28] and the latter to be estimated based on seismic microzonation). The parameters $\theta = e^{\mu}$, i.e., the median of PGA values, and β, i.e., the logarithmic standard deviation, are obtained based on a typological classification and refer to a very heavy-damage LS (DS4 in [26] and in [27]). These parameters are summarized, for these interfering elements and all others descripted hereinafter, in the Supplementary File accompanying this paper. For unreinforced masonry buildings [26], the typological class depends on regular/irregular masonry geometric bond pattern, flexible/rigid floors, presence of tie rods/tie beams, mixed structures, and number of stories above ground. For reinforced concrete buildings [27], the typological class depends on gravity-loads or earthquake-loads design, date of construction, and number of stories above ground. The typological class can be identified by means of visual surveys, for example, from web-based tools such as Google Street View, inasmuch as its characteristics are basic. An earthquake-resistant design can be inferred both from visual survey (beam size relative to column size, infill details, connections of tie rods with contrast plates, and so on) and by comparing the date of the first seismic site classification in the municipality/district with that of the building construction; the latter can be estimated based on historical cadastral maps and aerial photos available on the web. Additional interfering building types, such as churches or schools [29–31], can be easily integrated in the model if their fragility curves are available.

3.2. Fragility Curves for Bridges

In the road blockage risk assessment due to earthquakes, bridges are considered the most vulnerable elements [8]. The fragility curves of unreinforced masonry bridges are lognormally distributed and are a function of $a_g S$, as already defined. The parameters θ and β were analytically derived for single-span bridges by Zampieri et al. [32] depending on the raise/span ratio and arch thickness/span length ratio (from SC1 to SC9). The fragility

parameters reported in the Supplementary File accompanying this paper were selected referring to the second LS out of three (PL2 in [32]). The typological class can be again identified by means of visual surveys or from web-based tools such as Google Street Earth. To the authors' knowledge, no study on the fragility of typological classes of reinforced concrete Italian bridges is available. For this reason, the curves proposed for highway bridges in USA are used ([33], Sections 3.3.1.1 and 7.1.4-8 therein), which are based on the analytical work by Mander [34] and the references therein. Therein, two damage-state probabilities were identified: one for ground shaking (GS) and the other for ground failure (GF). Fragility curves are lognormally distributed functions of the ordinate of the pseudo-acceleration spectrum at a period of vibration of one second (S_e (T = 1 s)) in the case of GS and function of the maximum ground displacement d_g in the case of GF. Both S_e (T = 1 s) and d_g can be obtained from the Italian building code where seismic hazard is defined [28]. Each curve is characterized by a median value of GS or GF and an associated dispersion factor (lognormal standard deviation). The HAZUS technical manual proposes 28 primary bridge classes with four damage states and 224 bridge damage functions, of which 112 are due to GS and 112 to GF. The medians are indicated in a specific table, and the dispersion is set to 0.6 for GS and 0.2 for GF (refer to the Supplementary File accompanying this paper). The selected damage state for the interruption of the road is the extensive damage (ds4), defined by any column degrading without collapse-shear failure, significant residual movement at connections, or major settlement approach, vertical offset of the abutment, differential settlement at connections, or shear key failure at abutments.

The fragility median due to GS is modified by two factors as follows:

$$\exp(\mu_{GS,new}) = \exp(\mu_{GS}) \cdot K_{3D} \cdot K_{skew} \quad (2)$$

K_{3D} is a coefficient function that modifies the pier bidimensional capacity to allow for the tridimensional arch action in the deck depending on the number of spans (refer to the Supplementary File accompanying this paper); K_{skew} is a coefficient function of skew angle α, defined as the angle between the centerline of a pier and a line normal to the roadway centerline:

$$K_{skew} = \sqrt{\sin(90 - \alpha)} \quad (3)$$

The modified fragility median due to GF is as follows:

$$\exp(\mu_{GF,new}) = \exp(\mu_{GF}) \cdot f_1 \quad (4)$$

f_1 is a modification factor that is a function of the number of spans, width of the span, and length and skewness of the bridge. As discussed for the fragility curves of buildings, the geometrical information necessary for the classification of bridges can be estimated from Google Street View, and the global measures can be obtained from open-source tools such as Google Earth. Finally, the procedure requires the calculation of a combined probability of exceedance of the LS, starting from the two damage-state probabilities ([33] Section 5.6.3):

$$p_{comb} = p_{GS} + p_{GF} - p_{GS} \cdot p_{GF} \quad (5)$$

3.3. Fragility Curves for Retaining Walls

The fragility curves for retaining walls are those obtained analytically by Argyroudis et al. [35]. The log-normally distributed curves are a function of the free-field acceleration on bedrock a_g and of soil categories C and D in the Italian building code [36]. The soil categories can be assumed from seismic microzonation studies and brought back to the two considered in the model. The exponential median and the dispersion are diverse for different wall geometries (refer to the Supplementary File accompanying this paper). Hereinafter, it is assumed as a level of performance of the retaining wall significant for road blockage of the third damage state (DS3 in [35]), which is the most severe. It is worth noting

that these fragility curves refer to a rigid rotation of the wall and not to a disintegration of masonry, unfortunately observed during the 2016 seismic event [37].

3.4. Fragility Curves for Slopes

The fragility curves for slopes used in the path analysis are those analytically obtained by Wu [38]. Whereas in the original work, a specific seismic coefficient was defined, here and in the Supplementary File accompanying this paper, the lognormally distributed curves are expressed as a function of the maximum ground acceleration a_gS. The median and the dispersion are diverse for rocky slopes (wedge sliding) and soft slopes (sliding along a planar surface) and depend on the inclination angle of the slope. Angles less than 15° are neglected, in analogy to what is assumed for the topographic categories in the Italian building code [36]. The inclination angle can be estimated by means of cross-sections obtained from programs such as Google Earth. However, more reliable estimations of the fragility curves can be obtained if additional data are available [39].

3.5. MAF for Individual Structures along the Path

The MAF of exceedance of the blockage LS for the j-th interfering element $\lambda_{LS,j}$ is given by the following expression ([40], Section 2.6.1):

$$\lambda_{LS,j} \cong \sum_{i=1}^{n} p_{LS}(im_i)\left|\Delta\overline{\lambda_i}\right| \tag{6}$$

where n is the number of the return periods considered in the site hazard curve, which is equal to nine in the Italian building code hazard [28]. $p_{LS}(im_i)$ is the probability of exceedance of the considered LS conditioned to the level im_i of the intensity measure adopted in the fragility curve (a_g, a_gS, $S_e(T = 1\,\mathrm{s})$, d_g). The probability $p_{LS}(im_i)$ is computed by means of the standardized cumulative distribution function as follows:

$$p_{LS}(im_i) = p(Y_{LS} \geq 1 | IM = im_i) \therefore p\left(S_{Y_{LS}=1} \leq IM = im_i\right) = \Phi\left(\frac{im_i - \mu_{\ln S_Y=1}}{\beta_{\ln S_Y=1}}\right) \tag{7}$$

in which $\mu_{\ln S_Y=1}$ is the mean and $\beta_{\ln S_Y=1}$ is the standard deviation of the logarithm of the intensity S_Y = 1 that causes the attainment of the LS $(Y_{LS} = 1)$. The frequency λ_i is the MAF of exceedance of the level im_i of the considered intensity measure, while $\left|\Delta\overline{\lambda_i}\right|$ is its variation between consecutive return periods.

3.6. MAF for an Entire Path and for a Network of Paths with Same Start and End Points

The MAF of exceedance of the LS of the blockage of an entire road segment $\lambda_{LS,s}$ is calculated considering an in-series system [8]:

$$\lambda_{LS,s} = 1 - \prod_{j=1}^{ie}\left(1 - \lambda_{LS,j}\right) \tag{8}$$

where ie is the number of interfering elements along the path. The MAF of exceedance of the LS of blockage of the segment increases with the increment of ie and is larger than the largest frequency of all the elements along the segment.

For what concerns a network of paths with a unique starting point and a unique end point, the MAF of exceedance considering an in-parallel system with redundant segments $\lambda_{LS,rs}$ reads as given [41]:

$$\lambda_{LS,rs} = \prod_{j=1}^{ie}\lambda_{LS,j} \tag{9}$$

This way, with a small increase in the computational effort, one can consider the redundancy of the path that implies, at least in some road sections, alternative paths.

4. Application of the Proposed Methodology to Amatrice (Italy)

4.1. Description of the Case Study

Amatrice is the municipality mostly hit by the 24 August 2016 Central Italy earthquake, with 229 deaths out of a total number of 299 deaths in the whole affected area. According to the 2001 ISTAT (Italian National Institute of Statistics) census in the municipality, there were 2633 residents, but the actual exposure was largely higher due to a festival at the time of the seismic event. In a list disseminated by the local prefecture on 2 September 2016, approximately 59% of victims were not residents. The high number of deaths was also due to the significant earthquake intensity [42] and to the high vulnerability of buildings [43].

Although the performance of the bridges affected by the 2016 earthquake was investigated in [44], the overall response of the Amatrice road network in terms of its interaction with buildings, retaining walls, and slopes has not been studied so far (Figure 4). To better understand its impact, it is worthwhile to give details on the distribution of the population in the municipality. According to the 2001 census, the resident population was subdivided into 49 settlements with a municipal area of 174 km^2 (Figure 4). The vast majority of buildings was used as vacation housing. Such a widespread territorial organization is not an exception in the Apennines mountain range: for instance, L'Aquila has 19 settlements [26], Accumoli 17, Leonessa 35, Rieti 10, and Lucoli 15. Therefore, it is evident that the road blockage risk assessment is an issue of primary relevance. In many settlements as well as in the main one of Amatrice, the buildings are built along the road network, representing for it an external risk. Other interfering elements are bridges, retaining walls, and slopes. Additionally, emergency and civil protection services were all located in the main settlement, for example, the town hall, hospital, police station, school, sports hall, and sports ground. Assessing the seismic risk associated with paths starting from a minor settlement and arriving to the main settlement is then essential for the safety of people and to properly guarantee social services.

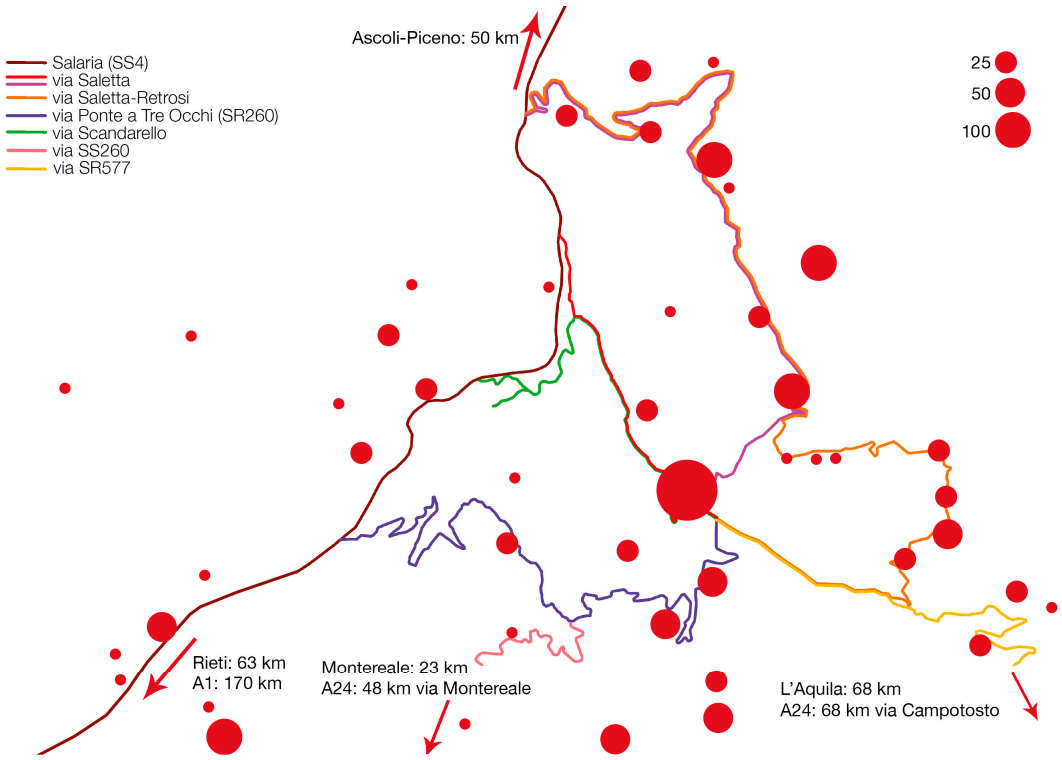

Figure 4. Amatrice municipality: network of roads and distribution of resident population. (The largest circle is out of scale and corresponds to the Amatrice settlement, having about 1000 residents).

4.2. Analysis Steps and Selection of the Paths

To make the proposed procedure understandable, a simplified yet explanatory scenario with two alternative paths based on three road segments is shown in Figure 5.

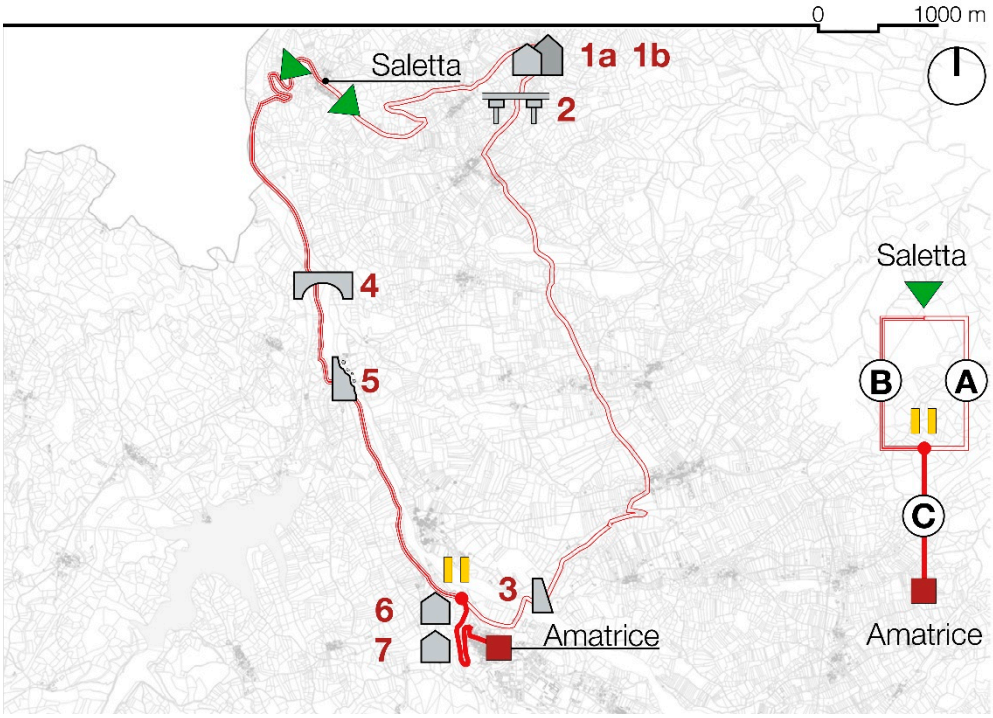

Figure 5. Selected paths in the Amatrice area.

The process steps applied to the case study are the following:

1. Identification of the starting point: Here, Saletta, one of the most populous settlements in the municipality and, in the meanwhile, quite far away from the end point (around 10 km), is assumed as the starting point;
2. Identification of the end point: Here, the Amatrice settlement, where all the main public functions are concentrated, is assumed as the ending point;
3. Identification of the possible paths connecting the starting and end points;
4. Identification of some illustrative interfering elements along the road segments and their classification according to the typological classes defined in Section 3, each of which has its own fragility curve;
5. Definition of the seismic demand relevant for each interfering element [28];
6. Calculation of the MAF of exceedance of the blockage LS of the road for each single element;
7. Calculation of the MAF of exceedance of the blockage LS of the entire path.

Regarding step #2, as displayed in Figure 5, just two possible paths as a combination of three segments are considered: Segment A and segment B are alternative, while segment C is an obligatory passage. Although the actual road configuration between Saletta and Amatrice is more articulated, the selected paths and segments are sufficient to illustrate the main features of the proposed procedure. As for step #3, along the segments are many interfering elements, but here, only some illustrative ones are considered. They are much fewer than those that actually exist but are representative for the application of the procedure (Figure 5):

- Segment A: two unreinforced masonry buildings, a reinforced concrete bridge, and a retaining wall;
- Segment B: an unreinforced masonry bridge and a slope;
- Segment C: an unreinforced masonry building and a reinforced concrete building.

Regarding step #4, in the ShakeMap referring to the 24 August 2016 event (https://shakemap.rm.ingv.it/shake4/viewLeaflet.html?eventid=7073641 (accessed on 30 March 2024)), the difference between the maximum acceleration of two relatively distant settlements, such as Saletta and Amatrice, was less than 8%. Therefore, it is reasonable to consider for all interfering elements a uniform base hazard, such as that of the main settlement derived by the Italian building code hazard [28], instead of scenario analyses, which on the contrary are necessary for large territorial studies [9]. In this way, the procedure remains manageable for small technical offices, which are already familiar with the code-based seismic hazard assessment. Nonetheless, seismic demand at each interfering element can be adjusted for specific site conditions estimated from microzonation studies. The amplification zones therein can be led back to the categories B, C, and D as defined in the Italian building code [36]. This way, one can exploit the basic spectra of the nine return periods available in the Italian code (Table 1), whereas the amplification factors in microzonation studies are usually estimated for only one return period. Depending on the considered interfering element type, the site category will modify the intensity measure (peak ground acceleration, spectral acceleration, and peak ground displacement) or will determine the selection of a specific fragility curve (as in the case of retaining walls).

Table 1. Local seismic base hazard of Amatrice according to the Italian building code hazard [28] and intensity measures relevant to the case study.

T_R	λ	Δλ	a_g	F_o	T_C^*	a_gS (B)	a_gS (C)	S_a (1.0 s; C)	PGD (C)
Years	**1/Years**	**1/Years**	**g**	**-**	**s**	**g**	**G**	**G**	**cm**
30	0.0333	0.0133	0.078	2.393	0.273	0.094	0.117	0.123	2.412
50	0.0200	0.0097	0.103	2.324	0.280	0.124	0.155	0.161	3.411
72	0.0139	0.0050	0.122	2.311	0.287	0.146	0.182	0.192	4.246
101	0.0099	0.0034	0.141	2.295	0.294	0.170	0.212	0.225	5.208
140	0.0071	0.0025	0.163	2.293	0.302	0.195	0.240	0.260	6.249
201	0.0050	0.0025	0.189	2.310	0.315	0.227	0.272	0.304	7.598
475	0.0021	0.0020	0.259	2.362	0.342	0.299	0.345	0.417	11.398
975	0.0010	0.0009	0.332	2.399	0.360	0.359	0.406	0.515	15.417
2475	0.0004	0.0006	0.450	2.459	0.381	0.450	0.466	0.630	21.373

As explained in Section 2.2, the MAF calculated at step #7 is compared to an upper limit of acceptable MAF for the road blockage LS, which is assumed equal to $7.0 \cdot 10^{-4}$ for each interfering element. In addition, this MAF is compared to the MAF of an alternative solution considering two scenarios:

1. The strengthening of an unreinforced masonry building and of a reinforced concrete building along the path, which reduces the associated seismic risk;
2. An alternative path overriding some elements/hypothesizing to demolish them.

Each road segment is described in detail in the following subsections, and the fragility data are derived for each interfering element and the associated risk.

4.3. Path n.1—Segment A

Segment A is characterized by the presence of two unreinforced masonry buildings, a reinforced concrete bridge, and a retaining wall. The two unreinforced masonry buildings are facing one another; the road width is equal to 3.5 m. The two buildings are approximately 5 and 7 m tall (Figure 6); therefore, the condition expressed in Equation (1) is satisfied: $\frac{h_{b1}+h_{b2}}{w} = \frac{5+7}{3.5} = 3.4 > 1.0$. Thus, the buildings interfere with the path and must be considered in the road blockage risk assessment.

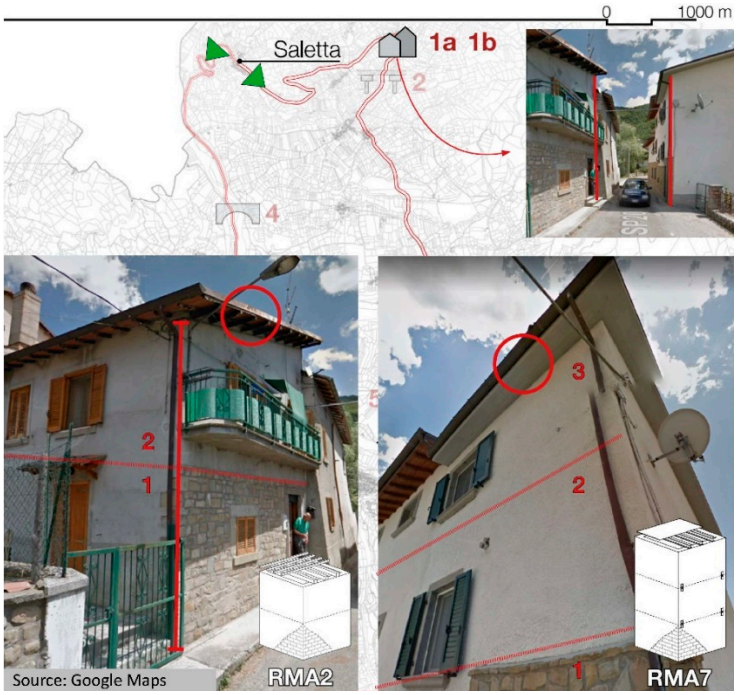

Figure 6. Buildings 1a and 1b on road segment A. Numbers identify stories, circles highlight the type of roof.

Building 1a (see numbers in Figure 5) is made of masonry with a regular geometric bond pattern and a timber floor/roof, without tie rods/ring beams, and has two stories; therefore, it falls under the class RMA2 [26], to which e^{μ} = 5.65 g and β = 1.82 ln(g) correspond (for readiness, refer to the Supplementary File accompanying this paper). The building stands on a type C soil; the relevant intensity measure for this element is $a_g S$ and accounts for the site conditions [24] (see Table 2). The probability of exceedance of the severe-damage LS (DS4) for the first return period (30 years) characterized by $a_g S$ = 0.117 g is as follows:

$$p_{SL}\left(im_{i=1(T_R=30y)}\right) = \Phi\left(\frac{\ln 0.117 - \ln 5.65}{1.82}\right) = 0.01656 \quad (10)$$

Table 2. Calculation of probability for the individual return period and of the MAF for Building 1a in road segment A.

a_gS (C)	$p_{SL}(s_i)$	$\Delta\lambda_i$	$\lambda_{LS,j}$
g	**-**	**1/Year**	**1/Year**
0.117	0.01656	0.01333	0.00022
0.155	0.02400	0.00972	0.00023
0.182	0.02959	0.00505	0.00015
0.212	0.03562	0.00337	0.00012
0.240	0.04139	0.00246	0.00010
0.272	0.04770	0.00252	0.00012
0.345	0.06223	0.00197	0.00012
0.406	0.07390	0.00085	0.00006
0.466	0.08522	0.00062	0.00005
		Sum (Equation (6))	0.00118

Such a calculation must be repeated for all the return periods, obtaining the values of the second column of Table 2. Afterwards, Equation (6) applies, in which the increments of MAF listed in the third column of Table 2 are considered. The MAF of exceedance is approximately equal to $11.8 \cdot 10^{-4}$, which is higher than the threshold value of $7.0 \cdot 10^{-4}$, showing the high risk associated with this element. In fact, the MAF value is reminiscent of the comparatively high vulnerability shown by unreinforced masonry buildings during the 2009 L'Aquila, Italy earthquake, whose data are at the base of the fragility curves reported in [26].

Building 1b (Figure 6) is a three-story, regular bond pattern, unreinforced masonry construction with reinforced concrete floors, a roof, and ring beams; for these reasons, it falls under the class RMA7. Considering the mean and standard deviation values of the corresponding fragility function [26] (for readiness, refer to the Supplementary File accompanying this paper) and developing the same calculations made for Building 1a, the MAF of exceedance of the severe-damage LS is $3.4 \cdot 10^{-4}$. This value is lower than the threshold; therefore, the element is safe against that LS. Apparently, one should expect for Building 1b a smaller MAF than that of Building 1a, as e^{μ} is equal to 5.65 g for the former and 3.94 g for the latter. Nevertheless, as the standard deviation of Building 1b (β = 1.26 ln(g)) is less than that of Building 1a (β = 1.82 ln(g)), the final MAF of the latter is larger.

Along the path, the other interfering elements (elements #2 and #3 in Figure 5) are a single-span reinforced concrete bridge and a 6 m tall retaining wall (MS1), both standing on a type C soil. The reinforced concrete bridge, built in the settlement of Cossito (Figure 7a), is considered to be earthquake-resistant because the first seismic classification of Amatrice dates back to 1915, and the structure was constructed after that date. The bridge has a single span (Figure 7b) and is less than 150 m long; therefore, its class is HWB4. The skew angle is zero, and therefore, the corresponding coefficient K_{skew} is unitary (Equation (3)).



Figure 7. Cossito reinforced concrete bridge of Path n.1—Segment A: (**a**) plan (#2 in Figure 5) and (**b**) photograph (number highlights single span).

The following parameters are obtained from [33] (and can be found in the Supplementary File accompanying this paper):

- K_{3D} = 1.33;
- $\exp(\mu_{GS})$ = 1.20 g, β = 0.6 (GS);

- $\exp(\mu_{GF}) = 0.1$ m, $\beta = 0.2$ (GF);
- $f_1 = 1$.

The modified fragility median due to GS is then as follows:

$$\exp(\mu_{GS,new}) = \exp(\mu_{GS}) \cdot K_{3D} \cdot K_{skew} = 1.2\ \text{g} \cdot 1.33 \cdot 1 = 1.596\ \text{g} \quad (11)$$

The modified fragility median due to GF is as follows:

$$\exp(\mu_{GF,new}) = \exp(\mu_{GF}) \cdot f_1 = 0.1 \cdot 1 = 0.1\ \text{m} \quad (12)$$

Equation (5) applies for computing the combined probability of exceedance of the LSs for GS and GF. It is observed that the probability for ground failure plays a more relevant role than that of ground shaking. The resultant MAF of the reference LS is $32.4 \cdot 10^{-4}$, which is almost three times greater than that of Building 1a. The bridge is therefore prone to the exceedance of the extensive damage LS; nevertheless, if one assumes a median of 0.35 m for the ground failure (threshold assumed in [33] for the complete-damage LS) rather than 0.10 m as for the extensive damage, the MAF of exceedance would decrease to $1.1 \cdot 10^{-4}$ less than the assumed capacity value of $7.0 \cdot 10^{-4}$.

The retaining wall (Figure 8a) is 6 m tall and falls in the category MS1, for which $e^{\mu} = 1.02$ g and $\beta = 0.7\ \ln(g)$ (refer to the Supplementary File accompanying this paper). The resultant MAF of exceedance of the reference LS is $2.2 \cdot 10^{-4}$, which is less than the capacity value.



(**a**) (**b**)

Figure 8. (**a**) Retaining wall of Path n.1—Segment A; (**b**) reinforced concrete building in segment C (source: Google Maps).

With the calculated MAFs, Equation (8) can be used to compute the MAF of exceedance of the LS of interruption of the entire segment $\lambda_{LS,A}$ (Table 3):

$$\lambda_{LS,A} = 1 - \left(1 - 11.8 \cdot 10^{-4}\right) \cdot \left(1 - 3.4 \cdot 10^{-4}\right) \cdot \left(1 - 32.4 \cdot 10^{-4}\right) \cdot \left(1 - 2.2 \cdot 10^{-4}\right) = 49.8 \cdot 10^{-4} \quad (13)$$

Table 3. MAF of the single structures in the road segments and of the entire path.

Segment A		
Element	$\lambda_{LS,j}$	$1 - \lambda_{LS}$
1a	0.00118	0.99882
1b	0.00034	0.99966
2	0.00324	0.99676
3	0.00022	0.99978
System	0.00498	0.99502

Table 3. *Cont.*

Segment B		
Element	$\lambda_{LS,j}$	$1 - \lambda_{LS}$
4	0.00787	0.99213
5	0.00095	0.99905
System	0.00881	0.99119
Segment C		
Element	$\lambda_{LS,j}$	$1 - \lambda_{LS}$
6	0.00260	0.99740
7	0.00474	0.99526
System	0.00733	0.99263

4.4. Path n.2—Segment B

Segment B is characterized by the presence of an unreinforced masonry bridge and a slope. The bridge (element #4 in Figure 5) stands on a type B soil and has a single span of 12.0 m and a structural thickness of 0.6 m. With these characteristics, it can be classified as class SC9, to which $e^{\mu} = 0.20$ g and $\beta = 0.25\ \ln(g)$ correspond [32] (for readiness, refer to the Supplementary File accompanying this paper). The resultant MAF of exceedance of the reference LS is $78.7 \cdot 10^{-4}$. The slope (element #5 in Figure 5) stands on a type B soil, and its inclination angle is equal to 19°. It can be classified as class PR1, to which $e^{\mu} = 13.3$ g and $\beta = 2.27\ \ln(g)$ correspond [38] (refer to the Supplementary File). The resultant MAF of exceedance of the reference LS is $9.5 \cdot 10^{-4}$.

Repeating the same procedure as for road segment A, the MAF of exceedance of the LS of interruption of the entire segment $\lambda_{LS,B}$ is $88.1 \cdot 10^{-3}$ (Table 3). This high frequency of exceedance is mainly due to the high vulnerability of the unreinforced masonry bridge.

4.5. Path n.1 or 2—Segment C

Segment C does not have redundant alternatives and therefore is an obligatory passage. The road segment is characterized by the presence of a reinforced concrete building and an unreinforced masonry building (# 6 and #7 in Figure 5, both on type B soil). The road is 6 m wide and presents no other interfering element at the opposite side. The reinforced concrete building (Figure 8b) is 18 m tall; therefore, the condition expressed in Equation (1) is satisfied: $\frac{h_{b1}+h_{b2}}{w} = \frac{18+0}{6} = 3.0 > 1.0$. Similarly, the unreinforced masonry building is 9 m tall; hence, $\frac{h_{b1}+h_{b2}}{w} = \frac{9+0}{6} = 1.5 > 1.0$. Thus, the buildings interfere with the road and must be considered in the risk assessment. The reinforced concrete building (Figure 8b) has six stories and, despite its post-1915 construction date, cannot be considered earthquake-resistant because the columns are weaker than the beams, and short columns are present due to the infill arrangement. Consequently, the building can be classified as

class GD5 (generalized database), to which $e^{\mu} = 0.56$ g and $\beta = 0.83\ \ln(g)$ correspond [23] (for readiness, refer to the Supplementary File accompanying this paper). The resultant MAF of exceedance of the reference LS is $26.0 \cdot 10^{-4}$.

The three-story unreinforced masonry building has an irregular geometric bond pattern, flexible diaphragms, and no ring beams or ties. Therefore, its class is IMA6, for which $e^{\mu} = 0.86$ g and $\beta = 1.5\ \ln(g)$ (refer to the Supplementary File). The resultant MAF of exceedance of the reference LS is $47.4 \cdot 10^{-3}$.

Contrary to segments A and B, the MAF of exceedance of the interruption LS of the entire segment C reported in Table 3 is of no immediate use, except for comparison purposes, as shown later on.

The MAF of exceedance of the entire path is calculated considering first the two redundant segments and then the segment in common combined with them. As for the redundant segments, Equation (9), which is valid for an in-parallel system, applies:

$$\lambda_{LS,rs} = \prod_{j=1}^{s} \lambda_{LS,j} = \lambda_{LS,A} \cdot \lambda_{LS,B} = \left(49.8 \cdot 10^{-4}\right) \cdot \left(88.1 \cdot 10^{-4}\right) = 0.4 \cdot 10^{-4} \quad (14)$$

Afterwards, Equation (8), valid for an in-series system formed by the redundant segments A and B and by the buildings #6 and #7 insisting on segment C, applies to compute the MAF of the entire path:

$$\lambda_{LS,path} = 1 - \left(1 - 0.4 \cdot 10^{-4}\right) \cdot \left(1 - 26.0 \cdot 10^{-4}\right) \cdot \left(1 - 47.4 \cdot 10^{-4}\right) = 73.7 \cdot 10^{-4} \quad (15)$$

The results are synthetically reported in Table 4, and the procedure is graphically summarized in Figure 9.

Table 4. MAF of the paths.

Element	λ_{LS}	$1 - \lambda_{LS}$	λ_{lim}
1–5	0.00004	0.99996	
6	0.00260	0.99740	
7	0.00474	0.99526	
System	0.00737	0.99396	0.00559

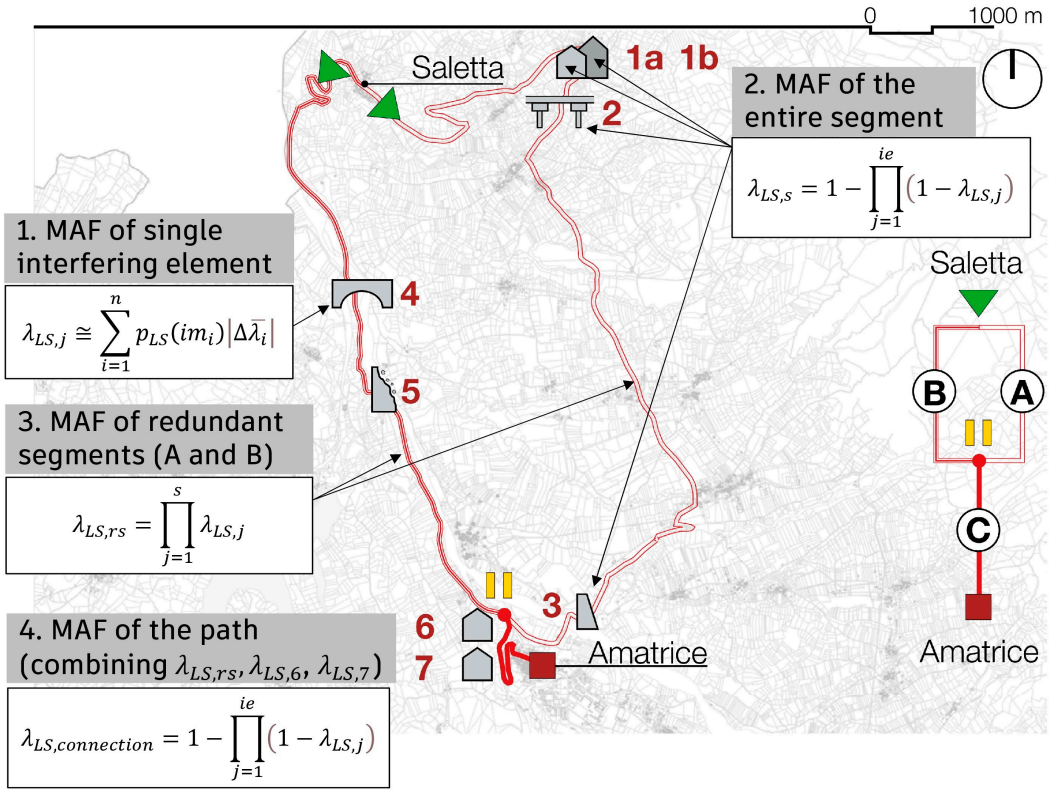

Figure 9. Procedure for the calculation of MAF for the entire connection.

There is only a small difference between the MAF of the entire connection and that of segment C alone (Table 3) because of the negligible MAF of exceedance of the in-parallel system A–B. In fact, if the path formed by segments A and C alone is considered, the MAF would be $122.7 \cdot 10^{-4}$, almost double that of the redundant path expressed in Equation (15).

This $73.7 \cdot 10^{-4}$ demand value must be compared with the limit MAF of the entire path assuming that all the elements along all its segments have a capacity threshold of $7.0 \cdot 10^{-4}$. Therefore, because along all segments there are eight interfering elements, the limit value of MAF is as follows:

$$\lambda_{lim} = 1 - \left(1 - 7 \cdot 10^{-4}\right)^{8} = 55.9 \cdot 10^{-4} \quad (16)$$

It is worth emphasizing that this limit (or capacity) value was calculated using only Equation (8) and considering only the total number of interfering elements present along all segments while disregarding if these segments are redundant or not. In this way, the presence of redundant segments determines a significant reduction in the demand but not in the capacity.

Nonetheless, in the case at hand, the resulting limit value in Equation (16) is less than the demand value in Equation (15); hence, the path is not safe. To satisfy the check, either a modification of the interfering element vulnerability or a road bypass is necessary, as discussed in the following section.

4.6. Reduction in Risk by Means of Seismic Strengthening or Bypass

Once the relevant authority verifies that the road path is unsafe, the safety level can be improved by reducing the demand value in terms of MAF. As explained in Section 2.2, such a reduction can be implemented by strengthening some elements of the path (preferably the most critical ones) or just bypassing them. To show a practical application of it, let us consider the example illustrated in the previous section.

Looking at Table 3, the maximum risk is observed for element #4 (unreinforced masonry bridge on segment B), for element #3 (reinforced concrete bridge on segment A), as well as for elements #6 and #7 (reinforced concrete and unreinforced masonry buildings on segment C). As the first ones are located in a redundant segment, one can disregard them and instead strengthen elements #6 and #7. Let us assume that building #6 is retrofitted to a current earthquake-resistant design. Consequently, the building can be classified as class SD5 post 1980, to which $e^{\mu} = 2.00$ g and $\beta = 0.83\ \ln(g)$ correspond [27] (for readiness, refer to the Supplementary File accompanying this paper). Similarly, building #7 is strengthened by stiffening its floors and improving the connections between structural members [45,46]. As a consequence, the building can be classified as class IMA7, to which $e^{\mu} = 1.33$ g and $\beta = 1.57\ \ln(g)$ correspond [26] (refer to the Supplementary File). The resultant MAFs of exceedance of the reference LS diminish to $9.0 \cdot 10^{-4}$ and $32.2 \cdot 10^{-4}$, determining a global MAF of exceedance of the entire path equal to $33.6 \cdot 10^{-4}$. This frequency is now lower than the limit value given by Equation (16).

If, for any reason, strengthening the elements along the path is not possible, the public authority could evaluate the opportunity of bypassing (or, equivalently, demolishing) some of them, for example, those of the last segment (C), by means of a new road layout. In this way, the MAF of exceedance of the entire path would be equal to that reported in Equation (14), equal to $0.4 \cdot 10^{-4}$. This value has to be compared with a frequency limit equal to $1 - \left(1 - 7 \cdot 10^{-4}\right)^6 = 41.9 \cdot 10^{-4}$, as the number of interfering elements in the path is now reduced to six. The scenario is therefore remarkably safe, as the demand is two orders of magnitude lower than the capacity value. Obviously, bypassing an entire road segment would imply economic, social, and time resources, which could be not compatible with the case under examination.

These calculations clearly show that the safety level of a road path can be remarkably improved through simple but sound tools that investigate different scenarios and quantify the benefits of retrofitting or bypassing interfering elements along the path. In the example, the analysis showed that the presence of a higher number of interfering elements associated with small MAFs is preferable to fewer elements with large MAFs. Moreover, the highest MAF is recorded for the non-redundant road segment C, which governs the order of magnitude of the other two segments demand. The three single segments have MAFs of the same order of magnitude, but when they are combined considering the effective road pattern, the MAFs diverge. It is sufficient to upgrade the two buildings on the non-redundant segment to achieve a safe condition: Such a solution would also imply higher safety for the users, not only regarding the road blockage. On the contrary, upgrading other structures or strengthening the slope in the other road segments would not bring any benefit in terms of road blockage risk.

The overall procedure can be effectively used for road safety planning by local authorities and road operators to quantify the safety level of local roads, especially in small and spread settlements. Such a tool would also support emergency preparedness challenges promoting awareness on the safest road paths to take in case of catastrophic events such as earthquakes.

5. Conclusions

This paper presents a novel method usable by managing entities to calculate the risk of a road path, possibly with redundant road segments, prone to blockage during an earthquake. The literature's fragility curves of typological classes of interfering elements, such as unreinforced masonry and reinforced concrete buildings, unreinforced masonry and reinforced concrete bridges, retaining walls, and slopes, were considered. Their median and dispersion values were used to calculate the probability of exceeding a blockage limit state (LS) of the road due to the failure of single elements. Then, the mean annual frequency (MAF) of exceedance of the blockage LS was calculated for segments and for the complete path (from start point to end point), displaying redundant segments. A practical example, located in the municipality of Amatrice, Italy, hit by the 2016 earthquake, was

illustrated. The presented method was revealed to be a simple but effective tool to estimate the current risk of the road network and to plan, if necessary, strengthening interventions on the interfering elements or bypassing some of them. The geometrical and mechanical information necessary to the classification of interfering elements can be estimated from open-source web-based tools, making the method easy and fast to apply also by a technical office with limited resources. Future studies may improve fragility curves by means of additional numerical analyses or empirical observations from recent earthquakes as well as by accounting for further interfering elements and classes, such as reinforced concrete arch bridges, retaining walls made of unreinforced masonry prone to disintegration, urban furniture, and abandoned vehicles.

Supplementary Materials: The following supporting information can be downloaded at: https://www.mdpi.com/article/10.3390/buildings14040984/s1, fragility curves of interfering elements: median and dispersion.

Author Contributions: Conceptualization, L.S.; methodology, L.S. and L.G.; software, L.S. and L.G.; formal analysis and investigation, L.S. and L.G.; resources, L.S.; writing—original draft preparation, L.G.; writing—review and editing, L.S. and L.G. All authors have read and agreed to the published version of the manuscript.

Funding: This work was partially carried out within the research project "SISMI Technologies for the safety improvement and the reconstruction of historical centres in seismic prone areas" sponsored by Latium regional government, and it was partially funded by the "Dipartimento di Protezione Civile—Consorzio RELUIS". The opinions expressed in this publication are those of the authors and are not necessarily endorsed by the funding bodies.

Data Availability Statement: The research data have been collected and made available in the Supplementary Material File.

Acknowledgments: The authors wish to thank: R. Amici (Municipality of Amatrice), F. Andreoli (Latium Road Company, ASTRAL), and F. Cola (Intermunicipal operative center, COI, of Accumoli-Amatrice) for valuable information about the performance of the elements interfering with the road network of the municipality of Amatrice. Additionally, the authors thank S. Perobelli for contributing to the figures in this manuscript.

Conflicts of Interest: The authors declare no conflicts of interest.

References

1. Hayes, J.L.; Biass, S.; Jenkins, S.F.; Meredith, E.S.; Williams, G.T. Integrating Criticality Concepts into Road Network Disruption Assessments for Volcanic Eruptions. *J. Appl. Volcanol.* **2022**, *11*, 8. [CrossRef]
2. Argyroudis, S.; Selva, J.; Gehl, P.; Pitilakis, K. Systemic Seismic Risk Assessment of Road Networks Considering Interactions with the Built Environment. *Comput.-Aided Civ. Infrastruct. Eng.* **2015**, *30*, 524–540. [CrossRef]
3. Bíl, M.; Kubeček, J.; Andrášik, R. An Epidemiological Approach to Determining the Risk of Road Damage Due to Landslides. *Nat. Hazards* **2014**, *73*, 1323–1335. [CrossRef]
4. El-maissi, A.M.; Argyroudis, S.A.; Nazri, F.M. Seismic Vulnerability Assessment Methodologies for Roadway Assets and Networks: A State-of-the-Art Review. *Sustainability* **2021**, *13*, 61. [CrossRef]
5. Anbazhagan, P.; Srinivas, S.; Chandran, D. Classification of Road Damage Due to Earthquakes. *Nat. Hazards* **2012**, *60*, 425–460. [CrossRef]
6. Yu, Y.C.; Gardoni, P. Predicting Road Blockage Due to Building Damage Following Earthquakes. *Reliab. Eng. Syst. Saf.* **2021**, *219*, 108220. [CrossRef]
7. Goretti, A.; Sarli, V. Road Network and Damaged Buildings in Urban Areas: Short and Long-Term Interaction. *Bull. Earthq. Eng.* **2006**, *4*, 159–175. [CrossRef]
8. Augusti, G.; Borri, A.; Ciampoli, M. Optimal Allocation of Resources in Reduction of the Seismic Risk of Highway Networks. *Eng. Struct.* **1994**, *16*, 485–497. [CrossRef]
9. Franchin, P.; Lupoi, A.; Pinto, P.E. On the Role of Road Networks in Reducing Human Losses after Earthquakes. *J. Earthq. Eng.* **2006**, *10*, 195–206. [CrossRef]
10. Zanini, M.A.; Faleschini, F.; Zampieri, P.; Pellegrino, C.; Gecchele, G.; Gastaldi, M.; Rossi, R. Post-Quake Urban Road Network Functionality Assessment for Seismic Emergency Management in Historical Centres. *Struct. Infrastruct. Eng.* **2017**, *13*, 1117–1129. [CrossRef]

11. Andreotti, C.; Liberatore, D.; Sorrentino, L. Identifying Seismic Local Collapse Mechanisms in Unreinforced Masonry Buildings through 3D Laser Scanning. In *Key Engineering Materials*; Trans Tech Publications Ltd.: Baech, Switzerland, 2015; Volume 628, pp. 79–84.
12. Costa, C.; Figueiredo, R.; Silva, V.; Bazzurro, P. Application of Open Tools and Datasets to Probabilistic Modeling of Road Traffic Disruptions Due to Earthquake Damage. *Earthq. Eng. Struct. Dyn.* **2020**, *49*, 1236–1255. [CrossRef]
13. Dhakal, S.; Cui, P.; Rijal, C.P.; Su, L.-J.; Zou, Q.; Mavrouli, O.; Wu, C.-H. Landslide Characteristics and Its Impact on Tourism for Two Roadside Towns along the Kathmandu Kyirong Highway. *J. Mt. Sci.* **2020**, *17*, 1840–1859. [CrossRef]
14. Sasabe, M.; Fujii, K.; Kasahara, S. Road Network Risk Analysis Considering People Flow under Ordinary and Evacuation Situations. *Environ. Plan. B Urban Anal. City Sci.* **2020**, *47*, 759–774. [CrossRef]
15. Takabatake, T.; Chenxi, D.H.; Esteban, M.; Shibayama, T. Influence of Road Blockage on Tsunami Evacuation: A Comparative Study of Three Different Coastal Cities in Japan. *Int. J. Disaster Risk Reduct.* **2022**, *68*, 102684. [CrossRef]
16. Ito, E.; Kawase, H.; Matsushima, S.; Hatayama, M. Tsunami Evacuation Simulation Considering Road Blockage by Collapsed Buildings Evaluated from Predicted Strong Ground Motion. *Nat. Hazards* **2020**, *101*, 959–980. [CrossRef]
17. *PrEN1998-1-1*; Eurocode 8—Design of Structures for Earthquake Resistance—Part 1-1: General Rules and Seismic Action (September 2022 Draft Version). The European Union: Maastricht, The Netherlands, 2022.
18. *PrEN1998-1-3*; Eurocode 8—Design of Structures for Earthquake Resistance—Part 1-3: Assessment and Retrofitting of Buildings and Bridges (July 2022 Draft Version). The European Union: Maastricht, The Netherlands, 2022.
19. Santarelli, S.; Bernardini, G.; Quagliarini, E. Earthquake Building Debris Estimation in Historic City Centres: From Real World Data to Experimental-Based Criteria. *Int. J. Disaster Risk Reduct.* **2018**, *31*, 281–291. [CrossRef]
20. Hirokawa, N.; Osaragi, T. Earthquake Disaster Simulation System: Integration of Models for Building Collapse, Road Blockage, and Fire Spread. *J. Disaster Res.* **2016**, *11*, 175–187. [CrossRef]
21. Moya, L.; Mas, E.; Yamazaki, F.; Liu, W.; Koshimura, S. Statistical Analysis of Earthquake Debris Extent from Wood-Frame Buildings and Its Use in Road Networks in Japan. *Earthq. Spectra* **2020**, *36*, 209–231. [CrossRef]
22. Lam, J.C.; Adey, B.T.; Heitzler, M.; Hackl, J.; Gehl, P.; van Erp, N.; D'Ayala, D.; van Gelder, P.; Hurni, L. Stress Tests for a Road Network Using Fragility Functions and Functional Capacity Loss Functions. *Reliab. Eng. Syst. Saf.* **2018**, *173*, 78–93. [CrossRef]
23. Lo, I.T.; Lin, C.Y.; Yang, C.T.; Chuang, Y.J.; Lin, C.H. Assessing the Blockage Risk of Disaster-Relief Road for a Large-Scale Earthquake. *KSCE J. Civ. Eng.* **2020**, *24*, 3820–3834. [CrossRef]
24. Anelli, A.; Mori, F.; Vona, M. Fragility Curves of the Urban Road Network Based on the Debris Distributions of Interfering Buildings. *Appl. Sci.* **2020**, *10*, 1289. [CrossRef]
25. CTMS Commissione Tecnica per La Microzonazione Sismica. *Manuale per L'analisi Della Condizione Limite per l'Emergenza (CLE) Dell'insediamento Urbano*; Dipartimento della Protezione Civile: Rome, Italy, 2014.
26. Zucconi, M.; Ferlito, R.; Sorrentino, L. Typological Damage Fragility Curves for Unreinforced Masonry Buildings Affected by the 2009 L'Aquila, Italy Earthquake. *Open Civ. Eng. J.* **2021**, *15*, 117–134. [CrossRef]
27. del Gaudio, C.; di Ludovico, M.; Polese, M.; Manfredi, G.; Prota, A.; Ricci, P.; Verderame, G.M. Seismic Fragility for Italian RC Buildings Based on Damage Data of the Last 50 Years. *Bull. Earthq. Eng.* **2020**, *18*, 2023–2059, Erratum in *Bull. Earthq. Eng.* **2020**, *18*, 4547–4548. [CrossRef]
28. Italian Ministry of Infrastructures and Transport. Norme Tecniche per le Costruzioni. DM 14/01/2008, Rome, Italy. 2008. Available online: https://www.gazzettaufficiale.it/eli/id/2008/02/04/08A00368/sg (accessed on 30 March 2024). (In Italian)
29. di Ludovico, M.; Digrisolo, A.; Graziotti, F.; Moroni, C.; Belleri, A.; Caprili, S.; Carocci, C.; Dall'Asta, A.; de Martino, G.; de Santis, S.; et al. The Contribution of ReLUIS to the Usability Assessment of School Buildings Following the 2016 Central Italy Earthquake. *Boll. Di Geofis. Teor. Appl.* **2017**, *58*, 353–376.
30. Sorrentino, L.; Alshawa, O.; Liberatore, D. Observations of Out-of-Plane Rocking in the Oratory of San Giuseppe Dei Minimi during the 2009 L'Aquila Earthquake. In *Proceedings of the Applied Mechanics and Materials*; Trans Tech Publications Ltd.: Wollerau, Switzerland, 2014; Volume 621, pp. 101–106.
31. Salzano, P.; Casapulla, C.; Ceroni, F.; Prota, A. Seismic Vulnerability and Simplified Safety Assessments of Masonry Churches in the Ischia Island (Italy) after the 2017 Earthquake. *Int. J. Archit. Herit.* **2022**, *16*, 136–162. [CrossRef]
32. Zampieri, P.; Zanini, M.A.; Faleschini, F. Derivation of Analytical Seismic Fragility Functions for Common Masonry Bridge Types: Methodology and Application to Real Cases. *Eng. Fail. Anal.* **2016**, *68*, 275–291. [CrossRef]
33. HAZUS FEMA. *Hazus–MH 2.1: Technical Manual*; Federal Emergency Management Agency: Washington, DC, USA, 2012.
34. Mander, J.B. *Fragility Curve Development for Assessing the Seismic Vulnerability of Highway Bridges*; ASCE: Reston, VA, USA, 1999.
35. Argyroudis, S.; Kaynia, A.M.; Pitilakis, K. Development of Fragility Functions for Geotechnical Constructions: Application to Cantilever Retaining Walls. *Soil Dyn. Earthq. Eng.* **2013**, *50*, 106–116. [CrossRef]
36. Italian Ministry of Infrastructures and Transport. Norme Tecniche per le Costruzioni. DM 17/01/2018, Rome, Italy. 2018. Available online: https://www.gazzettaufficiale.it/eli/gu/2018/02/20/42/so/8/sg/pdf (accessed on 30 March 2024). (In Italian)
37. Felice, G.; Liberatore, D.; de Santis, S.; Gobbin, F.; Roselli, I.; Sangirardi, M.; AlShawa, O.; Sorrentino, L. Seismic Behaviour of Rubble Masonry: Shake Table Test and Numerical Modelling. *Earthq. Eng. Struct. Dyn.* **2022**, *51*, 1245–1266. [CrossRef]
38. Wu, X.Z. Development of Fragility Functions for Slope Instability Analysis: Fragility Functions for Slope Instability Analysis. *Landslides* **2015**, *12*, 165–175. [CrossRef]

39. Martino, S.; Battaglia, S.; Delgado, J.; Esposito, C.; Martini, G.; Missori, C. Probabilistic Approach to Provide Scenarios of Earthquake-Induced Slope Failures (PARSIFAL) Applied to the Alcoy Basin (South Spain). *Geosciences* **2018**, *8*, 57. [CrossRef]
40. DT212. *Documento Tecnico 212. Istruzioni per La Valutazione Affidabilistica Della Sicurezza Sismica Di Edifici Esistenti*; Consiglio Nazionale delle Ricerche: Roma, Italy, 2013.
41. Augusti, G.; Ciampoli, M.; Frangopol, D.M. Optimal Planning of Retrofitting Interventions on Bridges in a Highway Network. *Eng. Struct.* **1998**, *20*, 933–939. [CrossRef]
42. Mollaioli, F.; AlShawa, O.; Liberatore, L.; Liberatore, D.; Sorrentino, L. Seismic Demand of the 2016–2017 Central Italy Earthquakes. *Bull. Earthq. Eng.* **2019**, *17*, 5399–5427. [CrossRef]
43. Fiorentino, G.; Forte, A.; Pagano, E.; Sabetta, F.; Baggio, C.; Lavorato, D.; Nuti, C.; Santini, S. Damage Patterns in the Town of Amatrice after August 24th 2016 Central Italy Earthquakes. *Bull. Earthq. Eng.* **2018**, *16*, 1399–1423. [CrossRef]
44. Durante, M.G.; di Sarno, L.; Zimmaro, P.; Stewart, J.P. Damage to Roadway Infrastructure from 2016 Central Italy Earthquake Sequence. *Earthq. Spectra* **2018**, *34*, 1721–1737. [CrossRef]
45. Casapulla, C.; Mousavian, E.; Argiento, L.; Ceraldi, C.; Bagi, K. Torsion-Shear Behaviour at the Interfaces of Rigid Interlocking Blocks in Masonry Assemblages: Experimental Investigation and Analytical Approaches. *Mater. Struct./Mater. Et Constr.* **2021**, *54*, 134. [CrossRef]
46. Giresini, L. Effect of Dampers on the Seismic Performance of Masonry Walls Assessed through Fragility and Demand Hazard Curves. *Eng. Struct.* **2022**, *261*, 114295. [CrossRef]

Disclaimer/Publisher's Note: The statements, opinions and data contained in all publications are solely those of the individual author(s) and contributor(s) and not of MDPI and/or the editor(s). MDPI and/or the editor(s) disclaim responsibility for any injury to people or property resulting from any ideas, methods, instructions or products referred to in the content.